# Catalysis of the Electrochemical Reduction of Carbon Dioxide by Iron(0) Porphyrins: Synergystic Effect of Weak Brönsted Acids

**Iqbal Bhugun, Doris Lexa,‡ and Jean-Michel Savéant***

*Contribution from Laboratoire d'Electrochimie Moléculaire, l'Université Denis Diderot, Paris 7, France, and Unité Associée au CNRS No. 438, 2 place Jussieu, 75251 Paris Cedex 05, France*

*Received October 12, 1995*[⊗]

**Abstract:** Addition of weak Brönsted acids such as 1-propanol, 2-pyrrolidone, and $CF_3CH_2OH$ triggers a considerable improvement of the catalysis of $CO_2$ reduction by iron(0) tetraphenylporphyrins. Both the catalytic currents and the life time of the catalyst increase without significant formation of hydrogen. Unprecedented values of the turnover numbers per hour can thus be reached. Carbon monoxide is the main product, while formic acid is formed to a lesser extent. The yield of formic acid counterintuitively decreases as the acidity of the acid synergist increases, becoming negligible with $CF_3CH_2OH$. Analysis of the reaction kinetics suggests that the action of the acid synergist is to stabilize the initial $Fe^{II}CO_2^{2-}$ carbenoid complex by hydrogen bonding. The formation of a doubly hydrogen-bonded complex opens the route to the cleavage of one of the two C−O bonds resulting in the formation of CO within the iron coordination sphere. The formation of formic acid involves a reaction pathway where the iron−$CO_2$ interactions are weaker. The effect of the acid synergist is an example of electrophilic assistance in a two-electron push−pull mechanism where pulling the electron pair out of the substrate by means of the synergist is as important as pushing electrons from the catalyst into the substrate. With $CF_3CH_2OH$, the production of CO is so fast that it commences to inhibit the catalytic reaction. This self-inhibition phenomenon can be satisfactorily modeled under the assumption that product adsorption on the electrode surface obeys a Langmuir equilibrium and that the covered portions of the surface are totally inactive toward reduction of the catalyst.

Carbon dioxide is very poorly reactive toward electron injection. The standard potential of the $CO_2/CO_2^{\cdot-}$ couple in an aprotic solvent such as *N*,*N*′-dimethylformamide (DMF) containing a countercation ($NEt_4^+$), not giving rise to strong ion pairing, is indeed as negative as −2.2 V vs SCE.[1] This is one reason why many potential catalysts of the electrochemical reduction of $CO_2$ have been investigated that would avoid the intermediacy of the $CO_2^{\cdot-}$ anion radical along the reaction pathway. Molecules particularly suited to this goal are reduced states of transition metal complexes where electron transfer to $CO_2$ and the ensuing chemical steps are anticipated to take place within the metal coordination sphere.[2,3] Another reason for investigating such chemical[4] catalysts is that they may lead to a better selectivity than the direct electrochemical reduction of $CO_2$ at inert electrodes, such as mercury and lead, which yields mixtures of oxalate, formate, and carbon monoxide (plus carbonate) in aprotic solvents[5] and formic acid in water.[6]

The transition metal $CO_2$ reduction catalysts that have received the most active attention are Ni and Co cyclams,[7] rhenium carbonyl,[8] rhodium, iridium, osmium,[9] and ruthenium bipyridine[10] complexes, although a detailed mechanism could not be established in most cases.

Iron(0) porphyrins have been shown to catalyze the electrochemical reduction of $CO_2$ in DMF.[3a] The catalytic efficiency and life time of this catalyst are however rather low. It was discovered later that these two parameters can be dramatically

‡ Present address: Laboratoire de Bioénergétique and Ingéniérie des Proteines, UPR CNRS 9036, 31 Chemin J. Aiguier, 13009 Marseille, France.

⊗ Abstract published in *Advance ACS Abstracts,* February 1, 1996.

(1) Lamy, E.; Nadjo, L.; Savéant, J.-M. *J. Electroanal. Chem.* **1977**, *78*, 403.

(2) (a) For reviews, see refs 2b,c and also the introductions of refs 3b,c. (b) Silvestri, G. In *Carbon Dioxide as a Source of Carbon*; Aresta, M., Forti, G., Eds.; NATO ASI Series, Ser. C; Reidel: Dordrecht, 1987, pp 339. (c) Collin, J. P.; Sauvage, J. P. *Coord. Chem. Rev.* **1989**, *93*, 245.

(3) (a) Hammouche, M.; Lexa, D.; Savéant, J.-M.; Momenteau, M. *J. Electroanal*. **1988**, 249, 347. (b) Hammouche, M.; Lexa, D.; Momenteau, M.; Savéant, J.-M. *J. Am. Chem. Soc.* **1991**, *113*, 8455. (c) Bhugun, I.; Lexa, D.; Savéant, J.-M. *J. Am. Chem. Soc.* **1994**, *116*, 5015.

(4) (a) There are two types of homogeneous catalyses of electrochemical reactions. In redox catalysis,[4b−d] the reduced form of the catalyst couple is merely an outersphere electron donor that shuttles electrons from the electrode to the substrate. This homogeneous electron transfer is subject to the same activation/ driving force limitations as the outer sphere electron transfer at an inert electrode. The very existence of a catalytic effect thus derives from a physical rather than a chemical process, namely, the dispersion of the electrons in the same three-dimensional space as the substrate instead of the two-dimensional availability of the electrons at the electrode surface.[4b−d] In chemical catalysis,[4b−d] the interactions between the reduced form of the catalyst and the substrate are more intimate, involving the transient formation of an addition product between the reduced form of the catalyst and the substrate before regeneration of the oxidized form of the catalyst. (b) Andrieux, C. P.; Dumas-Bouchiat, J.-M.; Savéant, J.-M. *J. Electroanal. Chem.* **1978**, *87*, 39. (c) Andrieux, C. P.; Savéant, J.-M. Electrochemical Reactions. In *Investigations of Rates and Mechanisms;* Bernasconi, C. F., Ed.; Wiley: New York, 1986; Vol. 6, 4/E, Part 2, pp 305. (d) Andrieux, C. P.; Hapiot, P.; Savéant, J.-M. *Chem. Rev.* **1990**, *90*, 723.

(5) (a) Kaiser, U.; Heitz, E. *Ber. Bunsen-Ges. Phys. Chem.* **1973**, *77*, 818. (b) Gressin, J. C.; Michelet, D.; Nadjo, L.; Savéant, J.-M. *Nouv. J. Chim.* **1979**, *3*, 545. (c) Formate comes from the reaction of the $CO_2$ anion radical with the water contained in the solvent. Oxalate prevails at high current densities. It results from the coupling of two anion radicals. CO is obtained at low current densitives and high concentrations of $CO_2$. Interestingly for the following discussion, CO results from an acid−base reaction where $CO_2$ plays the role of the acid and is responsible for the breaking of one C−O bond in the anion radical. In accord with the preceding mechanism, the production of oxalate up to quantitave yields has been achieved at the pilot scale.[5g] (d) Amatore, C.; Savéant, J.-M. *J. Am. Chem. Soc.* **1981**, *103*, 5021. (e) Amatore, C.; Savéant, J.-M. *J. Electroanal. Chem.* **1981**, *125*, 22. (f) Amatore, C.; Nadjo, L.; Savéant, J.-M. *Nouv. J. Chim.* **1984**, *8*, 565. (g) Fisher, J.; Lehmann, T.; Heitz, E. *J. Appl. Electrochem.* **1981**, *11*, 743.

(6) (a) Royer, M. E. *C. R. Acad. Sci*. **1870**, *70*, 731. (b) Cohen, A.; Jahn, S. *Ber. Dtsch. Chem. Ges*. **1904**, *37*, 2836. (c) Ehrenfeld, R. *Ber. Dtsch. Chem. Ges*. **1905**, *38*, 4138. (d) Russel, P. G.; Kovac, N.; Srinivasan, S.; Steinberg, M. *J. Electrochem. Soc.* **1977**, *124*, 1329.

0002-7863/96/1518-1769$12.00/0 © 1996 American Chemical Society

improved by addition of magnesium ions to the solution.[3b] Since then it has been found that other Lewis acid cations such as $Ca^{2+}$, $Ba^{2+}$, $Li^{+}$, and $Na^{+}$ also produce a similar effect.[11] The idea thus emerged that association between an electron donor catalyst and an electrophilic assisting synergist is required to achieve a satisfactory catalysis. The same idea was tested with a weak Brönsted acid leading to a spectacular enhancement of the catalytic current as described in a recent preliminary communication.[3c]

One purpose of the work described below was to investigate several other Brönsted acids so as to define the type of acids that are appropriate for obtaining such effects. Another goal was to establish the mechanism through which these acids act as synergists to the electron donor catalyst having in mind that such an analysis may serve as an illustrating example of electron push−pull catalysis in general. During the course of this work, we came across several systems where the synergist is so effective that the products start to inhibit the initial step of the catalytic process. Comprehension and modeling of this self-inhibition process thus appeared necessary to extract the mechanism from the electrochemical kinetic data.

## Results and Discussion

Cyclic voltammetry and preparative scale electrolysis at a mercury electrode were the two main tools we used to determine the nature and yields of the reduction products and the kinetics and mechanism of the catalytic process. In all experiments, the iron tetraphenylporphyrin (TPP) catalyst was introduced in the DMF solution as the $Fe^{III}Cl$ complex.

**Preliminary Cyclic Voltammetric Investigation.** Figure 1 shows a typical cyclic voltammogram of this complex in the absence of $CO_2$ as well as of proton donors. It exhibits three successive waves corresponding to the reversible formation of the Fe(II), $Fe(I)^{-}$, and $Fe(0)^{2-}$ complexes. Catalysis takes place at the $Fe(I)^{-}/Fe(0)^{2-}$ wave.[12] The formation of carbon monoxide can be detected on the reverse anodic trace of the voltammogram by the fact that it stabilizes the Fe(II) oxidation states at the expenses of $Fe(I)^{-}$ and Fe(III) and thus shifts the $Fe(I)^{-}$ oxidation wave in the negative direction and the Fe(II) oxidation wave in the positive direction.[3b] The magnitude of these changes, when observed on the reverse trace of the catalytic wave, thus provides a qualitative estimate of the catalysis efficiency for generation of CO. It cannot serve as a quantitative measure of CO production which requires, as for the other reduced species, a full analysis of the reaction products after preparative-scale electrolysis.

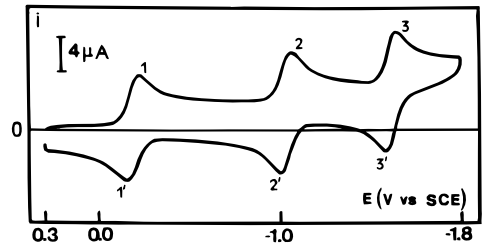


**Figure 1.** Cyclic voltammetry of $TPPFe^{III}Cl$ (1 mM) in DMF + 0.1 M $NEt_4ClO_4$ at a glassy carbon electrode. $T$ = 20 °C. Scan rate 0.1 = V/s.

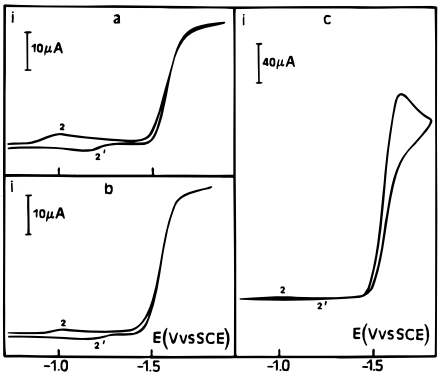


**Figure 2.** Cyclic voltammetry of $TPPFe^{III}Cl$ (0.5 mM) in DMF + 0.1 M $NEt_4ClO_4$ under 1 atm of $CO_2$ in the presence of 0.51 M 2-pyrrolidone (a), 6.66 M 1-propanol (b), and 1.47 M $CF_3CH_2OH$ (c). Mercury electrode, scan rate = 0.1 V/s. $T$ = 20°C. Scan rate = 0.1 V/s.

Under 1 atm of $CO_2$, but in the absence of any synergist, the $Fe(I)^{-}/Fe(0)^{2-}$ wave becomes irreversible and increases in height, albeit to a very modest extent (see Figure 2c in ref 3b or Figure 1b in ref 3c). These observations fall in line with the fact that, at preparative scale, catalysis is slow and leads to rapid destruction of the catalyst.

Figure 2 shows typical examples of the enhancement of the catalytic wave resulting from the addition of three different weak Brönsted acids: 2-pyrrolidone, 1-propanol, and $CF_3CH_2OH$.[13] Very large catalytic currents are observed in each case (compare their height with the peak current of the one-electron Fe(II)/$Fe(I)^{-}$ wave (2) in front). In all three cases the introduction of the acid triggers a drammatic increase of the catalytic current

(7) (a) Fischer, B.; Eisenberg, R. *J. Am. Chem. Soc.* **1980**, *102*, 7361. (b) Tinnemans, A. H. A.; Koster, T. P. M.; Thewissen, D. H. M. W.; Mackor, A. M. *Recl. Trav. Chim. Pays-Bas*. **1984**, *103*, 288. (c) Pearce, D. J.; Pletcher, D. *J. Electroanal. Chem*. **1986**, *197*, 317. (d) Beley, M.; Collin, J. P.; Ruppert, R.; Sauvage, J. P. *J. Chem. Soc., Chem. Commun.* **1984**, 1315. (e) Beley, M.; Collin, J. P.; Ruppert, R.; Sauvage, J. P. *J. Am. Chem. Soc.*, **1986**, *108*, 7461. (f) Collin, J. P.; Jouaiti, A.; Sauvage, J. P. *Inorg. Chem*. **1988**, *27*, 1986. (g) Fujihira, M.; Hirata, Y.; Suga, K. *J. Electroanal. Chem*. **1990**, *292*, 199. (h) Fujihira, M.; Nakmura, Y.; Hirata, Y.; Akiba, U.; Suga, K. *Denki Kagaku* **1991**, *59*, 532. (i) Balazs, G. B.; Anson, F. C. *J. Electroanal. Chem*. **1992**, *332*, 325. (j) Balazs, G. B.; Anson, F. C. *J. Electroanal. Chem*. **1993**, *361*, 149. (k) For a recent photochemical study of the reduction of $CO_2$ by cobalt macrocycle, see ref 7l. (l) Ogata, T.; Yanagida, S.; Brunschwig, B. S.; Fujita, E. *J. Am. Chem. Soc.* **1995**, *117*, 6708.

(8) (a) Hawecker, J.; Lehn, J. M.; Ziessel, R. *J. Chem. Soc., Chem. Commun*. **1983**, 536. (b) Hawecker, J.; Lehn, J. M.; Ziessel, R. *J. Chem. Soc., Chem. Commun*. **1984**, 328. (c) Hawecker, J.; Lehn, J. M.; Ziessel, R. *Helv. Chim. Acta* **1986**, *69*, 1990. (d) Sullivan, B. P.; Bolinger, C. M.; Conrad, D.; Vining, W. J.; Meyer, T. J. *J. Chem. Soc., Chem. Commun*. **1985**, 1414. (e) Breikss, A. I.; Abruna, H. D. *J. Electroanal. Chem*. **1986**, *209*, 101.

(9) (a) Bruce, M. R. M.; Megehee, E.; Sullivan, B. P.; Thorp, H. R.; O'Toole, T.; Downard, A.; Meyer, T. J. *Organometallics* **1988**, *7*, 238. (b) Bolinger, C. M.; Story, N.; Sullivan, B. P.; Meyer, T. J. *Inorg. Chem*. **1988**, *27*, 4582.

(10) (A) Ishida, H.; Tanaka, K.; Tanaka, T. *Chem. Lett*. **1985**, 405. (b) Ishida, H.; Tanaka, H.; Tanaka, K.; Tanaka, T. *J. Chem. Soc., Chem. Commun*. **1987**, 131. (c) Ishida, H.; Tanaka, K.; Tanaka, T. *Organometallics* **1987**, *6*, 181.

(11) Bhugun, I.; Lexa, D.; Savéant, J.-M. In preparation.

(12) (a) $Fe(0)^{2-}$ is one of the resonant forms of the complex where, starting from Fe(II), all the added electron density is located on the iron atom. Other possible resonant forms are the anion radical of $Fe(I)^{-}$ or the dianion of Fe(II), where the added electron density is shared between iron and the $\pi^*$ orbital of the porphyrin ring or entirely located in the latter, respectively. Although all three forms presumably contribute to the electronic structure of the complex, previous studies have shown that it is alkylated at the iron atom and not on the ring by alkyl halides[12b,c] and that it abstracts a bromonium ion from vicinal dibromides yielding the corresponding olefin.[12d,e] These observations demonstrate that reactions at $Fe(0)^{2-}$ may dominate the chemistry of this complex. A recent spectroscopic study, including Raman spectroscopy, has confirmed the importance of the $Fe(0)^{2-}$ resonant form.[12f] (b) Lexa, D.; Savéant, J.-M.; Wang, D. L. *Organometallics* **1986**, *5*, 1428. (c) Lexa, D.; Savéant, J.-M.; Su, K. B.; Wang, D. L. *J. Am. Chem. Soc.* **1988**, *110*, 7617. (d) Lexa, D.; Savéant, J.-M.; Su, K. B.; Wang, D. L. *J. Am. Chem. Soc.* **1987**, *109*, 6424. (e) Lexa, D.; Savéant, J-M.; Schäfer, H. J.; Su, K. B.; Vering, B.; Wang, D. L. *J. Am. Chem. Soc.* **1990**, *112*, 6162. (f) Anxolabéhère, E.; Chottard, G.; Lexa, D. *New J. Chem.* **1994**, *18*, 889.

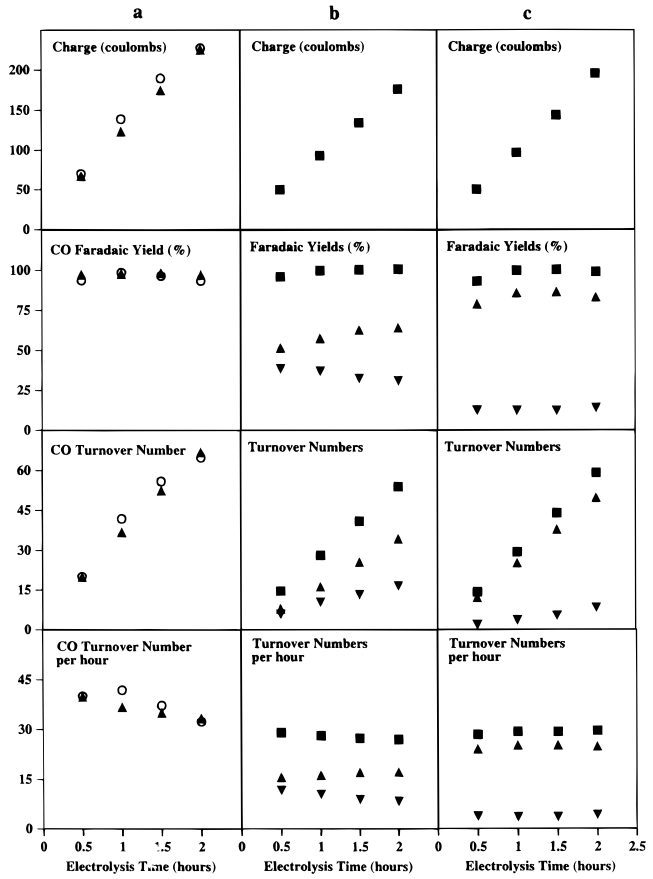


**Figure 3.** Electrolysis of $CO_2$ (1 atm) in the presence of TPPFeCl (1 mM) at a mercury pool cathode in DMF + 0.1 M $Et_4NClO_4$ (electrode potential, −1.7 V vs SCE; temperature, 20 °C) in the presence of (a) 0.55 M (○) and 1.37 M (▲) $CF_3CH_2OH$, (b) 6.7 M 1-propanol (▲, CO; ▼, $HCO_2^-$; ■, sum of products including $H_2$ and oxalate; see text), and (c) 6.3 M 1-propanol + 2.8 M $H_2O$ (▲, CO; ▼, $HCO_2^-$; ■, sum of products including $H_2$ and oxalate; see text).

(compare the current heights in Figure 2 to the current height in Figure 1b of ref 3c). It is observed that the efficiency of the acid synergist follows its acidity. However the use of stronger and stronger acids for increasing $CO_2$ reduction catalysis may not be a proper strategy if the iron(0) porphyrin catalyzes the reduction of the acid proton into hydrogen. In the absence of $CO_2$, the addition of 2-pyrrolidone or 1-propanol, in concentrations where large catalytic currents are observed in the presence of $CO_2$, does not alter the reversibility of the Fe(II)/Fe(I)$^-$ wave showing that catalysis of hydrogen evolution is negligible. Under the same conditions, addition of $CF_3CH_2OH$ renders the Fe(II)/Fe(I)$^-$ wave irreversible with an increase in height, which is however very small in comparison with the catalytic current observed in the presence of $CO_2$ (compare Figure 1c of ref 3c to Figure 2c above). This is an indication that hydrogen evolution should be small as compared to $CO_2$ reduction as has been confirmed by the preparative-scale experiments described below. However with much stronger acids, such as $Et_3NH^+$ ($pK_a$ ca. 9[13]), catalysis of proton reduction is very strong leading to quantitative hydrogen formation,[14] thus leaving little room

(13) (a) The $pK_a$'s of these various acids are not known in DMF. From the approximate relationship between $pK_a$'s in DMF and DMSO ($pK_a^{DMF} = 0.55 + 1.05pK_a^{DMSO}$ [13b]) and from values measured in DMSO for these acids or similar acids,[13c,d] it can be estimated that the $pK_a$'s in DMF lie in the following order: 1-propanol > $H_2O$ > pyrrolidone > $CF_3CH_2OH$. The H-bonding properties of these compounds are expected to lie in the same order. (b) Clare, B. W.; Cook, D.; Ko, E. C. F.; Mac, Y. C.; Parker, A. J. *J. Am. Chem. Soc.* **1966**, *88*, 1911. (c) Kolthoff, I. N.; Chantooni, M. K.; Bhowmik, S. *J. Am. Chem. Soc.* **1968**, *90*, 23. (d) Bordwell, F. G. *Acc. Chem. Res.* **1988**, *21*, 496.

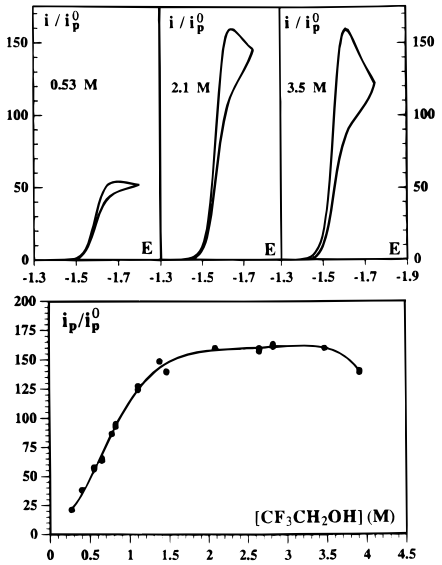


**Figure 4.** Cyclic voltammetry of the reduction of $CO_2$ (1 atm) in DMF + 0.1 M $Et_4NClO_4$ catalyzed by TPPFeCl (1 mM), variations with the concentration of added $CF_3CH_2OH$. Scan rate = 0.1 V/s. $T$ = 20 °C. $E$ = electrode potential vs aqueous SCE.

for $CO_2$ reduction. It is also worth noting that substantial formation of CO, as a result of catalysis, is apparent on all three voltammograms through the negative shift of the anodic wave 2′, due to stabilization of Fe(II) by CO.

**Preparative-Scale Electrolyses.** The results of preparative-scale electrolyses carried out under 1 atm of $CO_2$ in the presence of $CF_3CH_2OH$ or 1-propanol are summarized in Figure 3.

With $CF_3CH_2OH$ (Figure 3a), the reaction is selective, leading to the formation of more than 96% CO. No hydrogen, oxalate, or formate could be detected. The turnover number per hour slightly decreases with time as a result of a slow degradation of the porphyrin catalyst. Cyclic voltammetric analysis of the electrolyzed solutions revealed that the decay per catalytic cycle is 1% for [$CF_3CH_2OH$] = 0.55 M and 0.4% for [$CF_3CH_2OH$] = 1.37 M.

The reaction is less selective with 1-propanol (Figure 3b). Although CO remains the main product (∼60%), substantial amounts of formate are formed (∼35%). Small but detectable amounts of oxalate (1.6%) and hydrogen (4%) were also found among the reaction products. The deactivation of the catalyst, 2.2%/catalytic cycle, is faster than with $CF_3CH_2OH$.

The effect of water as a possible acid synergist[13] could not be investigated directly because its addition triggers the precipitation of the iron porphyrin. However this is not the case when a large amount of 1-propanol is already present in the solution. The results displayed in Figure 3c reveal that addition of water (2.8 M) to a solution already containing 6.3 M 1-propanol increases the CO yield up to 80% and diminishes the yield in formate down to 13%. The yields in oxalate and hydrogen also decrease (0.4% and 2%, respectively). It is also worth noting that the deactivation of the catalyst, now only 0.9%/catalytic cycle, decreases upon addition of water.

As a general trend, we thus observe, in the series of weak Brönsted acids comprising $CF_3CH_2OH$, water, and 1-propanol, that the selectivity of the reaction and the stability of the catalyst improve as the synergist becomes more acidic.[13]

**Kinetics and Mechanisms.** Addition of $CF_3CH_2OH$ triggers a considerable increase of the catalytic current. Figure 4 shows the variations of the voltammograms and the peak current as a function of the concentration of $CF_3CH_2OH$. The current, $i$,

(14) Bhugun, I.; Lexa, D.; Savéant, J.-M. Submitted.

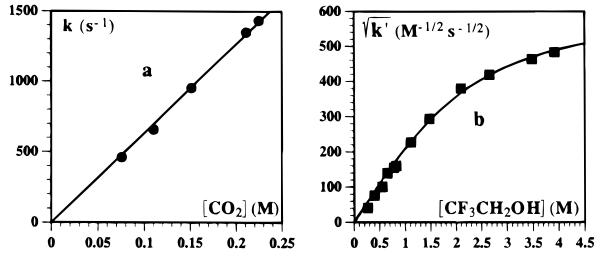


**Figure 5.** Kinetics of the catalysis of $CO_2$ reduction by TPPFeCl (0.96 mM) in DMF + 0.1 M $Et_4NClO_4$ at 20 °C, variation of the global rate constant with (a) $CO_2$ concentration ($[CF_3CH_2OH]$ = 0.4 M) and (b) $CF_3CH_2OH$ concentration under 1 atm of $CO_2$.

and peak current, $i_p$, are normalized toward the peak current, $i_p^0$, corresponding to one electron as obtained from the $Fe(I)^-/Fe(0)^{2-}$ wave in the absence of $CO_2$ and $CF_3CH_2OH$ (Figure 1). It is observed that $i_p/i_p^0$ increases with $[CF_3CH_2OH]$, reaching a limiting value at high concentrations. Simultaneously, the shape of the voltammogram changes from a S-shaped curve to a peak. The origin of the peak shape that progressively appears upon raising the $CF_3CH_2OH$ concentration will be discussed later. Up to 0.55 M $CF_3CH_2OH$, the voltammograms are close to the S-shaped curve, independent of scan rate, as defined by eq 1, which is expected when the substrate is in large excess over the catalyst and catalysis is not too fast so that the concentration of the substrate across the reaction layer is the same as its bulk concentration.[4cd,15]

$$\frac{i}{FS} = \frac{\sqrt{k}}{1 + \exp\left[\frac{F}{RT}(E - E^0)\right]} \qquad (1)$$

where $S$ is the electrode surface area, $E$ is the electrode potential, $E^0$ is the formal potential of the catalyst redox couple, and $k$ is the global pseudo-first-order rate constant of the catalytic process (AH = $CF_3CH_2OH$):

$$Fe(I)^- + e^- \rightleftharpoons Fe(0)^{2-} \qquad (0)$$

$$Fe(0)^{2-} + CO_2 + AH \xrightarrow{k} Fe(I)^- + \text{products}$$

The global rate constant $k$ is then immediately obtained from the height of the plateau current. The variation of $k$ with $CO_2$ concentration (Figure 5a) reveals that the reaction order in $CO_2$ is 1. From the variation of $k$ with $CF_3CH_2OH$ concentration, one can derive the variation of the pseudo-second-order rate constant $k' = k/[CO_2]$ (Figure 5b), using the previously determined $CO_2$ solubilities in DMF−$CF_3CH_2OH$ mixtures.[16] Within the considered range of $CF_3CH_2OH$ concentrations, the reaction order in $CF_3CH_2OH$ is 2.

These observations and the results of preparative-scale electrolyses suggest the mechanism depicted in Scheme 1. Following its electrochemical generation, the iron(0) complex combines with one $CO_2$ molecule to give a complex that we have represented by a single carbenoid resonant form. This representation is suggested by the fact that iron(II) complexes are strongly stabilized by CO, as seen earlier, and other carbene or carbenoid ligands.[17]

**Scheme 1**[a]

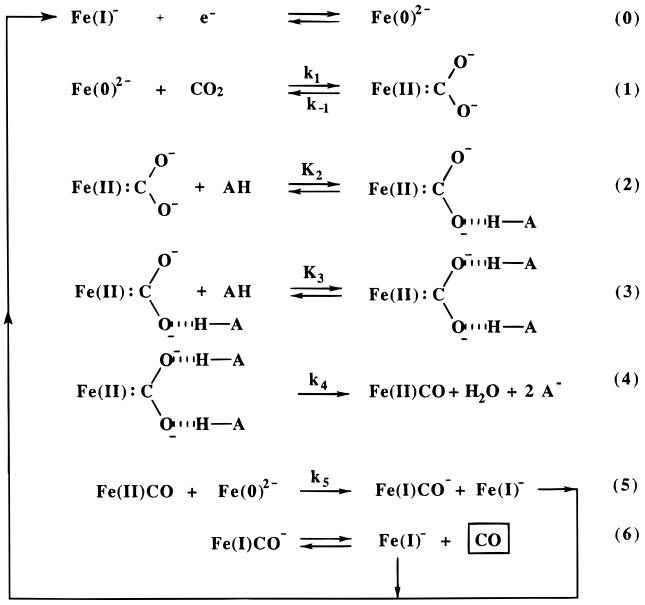


[a] $k$'s and $K$'s are the rate and equilibrium constants, respectively.

**Scheme 2**

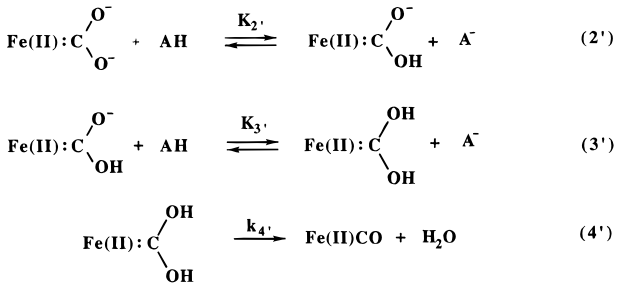


The addition of $CF_3CH_2OH$ stabilizes the carbenoid adduct through two successive addition equilibria (2 and 3) that are followed by the rate-determining cleavage of one C−O bond leading to the stable $Fe^{II}CO$ complex (4). The $Fe(I)^-$ catalyst is regenerated during the two last steps (5 and 6) by reduction of $Fe^{II}CO$.[18] Thus, within the considered range of $CF_3CH_2OH$ concentrations, the global rate constant $k$ is expressed as a function of the thermodynamic or kinetic characteristics of the successive steps by eq 2.

$$k = 2K_1K_2K_3k_4[CO_2][CF_3CH_2OH]^2 \qquad (2)$$

Scheme 1 is to be preferred to a reaction mechanism in which steps 2 and 3 would involve protonation of the carbenoid complex yielding successively two molecules of the conjugated alcoholate ($A^-$) as represented in Scheme 2. Indeed, such a mechanism would not be consistent with the S-shaped current−potential curves observed experimentally. As shown in the Supporting Information, they are peak-shaped as represented in Figure A1. According to Scheme 2, the voltammograms should be peak-shaped at low $CF_3CH_2OH$ concentration and

(15) (a) Savéant, J.-M.; Vianello, E. In *Advances in Polarography*; Longmuir, I. S., Ed.; Pergamon Press: London, 1960; pp 367−374. (b) Savéant, J.-M.; Su, K. B. *J. Electroanal. Chem.* **1984**, *171*, 341.

(16) Bhugun, I.; Lexa, D.; Savéant J.-M. *Anal. Chem.* **1994**, *66*, 3994.

(17) (a) Lexa, D.; Savéant, J.-M.; Battioni, J. P.; Lange, M.; Mansuy, D. *Angew. Chem., Int. Ed. Engl.* **1981**, *20*, 578. (b) Lange, M.; Battioni, J.-P.; Mansuy, D.; Lexa, D.; Savéant, J.-M. *J. Chem. Soc., Chem. Commun.* **1981**, *17*, 889. (c) Battioni, J. P.; Lexa, D.; Mansuy, D.; Savéant, J.-M. *J. Am. Chem. Soc.* **1983**, *105*, 207.

(18) (a) In step 5, the electron donor is regarded to be the iron(0) complex rather than the electrode itself. The competition between these two possible pathways ("DISP−ECE" competition) is governed by the parameter $(k_5/k^{3/2})(Fv/RT)^{1/2}$.[4c,18b] Over the whole series of experiments, the maximum value of $k$ is 5.8 $10^4$ $s^{-1}$. $k_5$ should be close to the diffusion limit ($10^{10}$ $M^{-1}$ $s^{-1}$). Thus for a catalyst concentration of 1 mM, the minimal value of the parameter, obtained for the lowest scan rate (0.1 V/s), 1.5, is still in favor of the DISP pathway with some contribution from the ECE pathway. The DISP pathway predominates more and more at lower $CF_3CH_2OH$ concentrations and higher scan rates. (b) Amatore, C.; Gareil, M.; Savéant, J.-M. *J. Electroanal. Chem.* **1983**, *47*, 1.

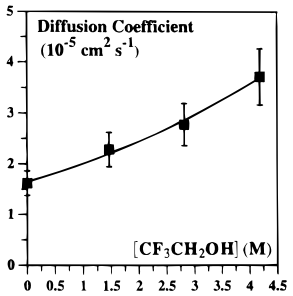


**Figure 6.** Variation of the diffusion coefficient of $CO_2$ with the concentration of $CF_3CH_2OH$ in DMF + 0.1 M $Et_4NClO_4$ solution.

become S-shaped upon raising the concentration as reaction 1 becomes the rate-determining step (see Supporting Information). These predictions are exactly opposite to the experimental observations, thus ruling out the occurrence of the mechanism depicted in Scheme 2.

What is thus the origin of the peak shape observed more and more markedly as the $CF_3CH_2OH$ concentration is raised? One possibility that ought to be examined is that it may result, in spite of the large bulk concentration of $CO_2$, from the fact that the catalysis rate becomes very large upon increasing the $CF_3CH_2OH$ concentration. Under such conditions, substrate diffusion tends to interfere in the control of the current and its concentration is no longer constant across the reaction layer. The factor that governs the consumption of the substrate in the reaction layer is $(RT/F)(k/v)(C_{cat}/C_{sub})(D_{cat}/D_{sub})$ ($v$ is the scan rate and $C$ and $D$ are the bulk concentrations and diffusion coefficients of the subscript species, respectively).[15b] The solubility of $CO_2$ in DMF−$CF_3CH_2OH$ mixtures has been determined previously at 20 °C and shown to vary from 0.228 to 0.168 M from pure DMF to pure $CF_3CH_2OH$.[16] The diffusion coefficient of the porphyrin was determined from the reversible the $Fe(I)^-/Fe(0)^{2-}$ cyclic voltammetric wave. It was found to be practically independent of the $CF_3CH_2OH$ concentration and equal to $3 \times 10^{-6}$ cm$^2$ s$^{-1}$. The diffusion coefficient of $CO_2$, determined by potential step chronoamperometry beyond the peak potential (at −2.45 V vs SCE) at 0.5 and 1 atm of $CO_2$ in the absence of porphyrin, increases with the $CF_3CH_2OH$ concentration as shown in Figure 6. Taking into account these variations, those of the $CO_2$ bulk concentrations, and the values of $k$ found at various $CF_3CH_2OH$ concentrations (see below), it was found that the consumption parameter is always <1.44. Simulation of the current−potential for this maximal value reveals the presence of a shallow peak. The ratio of the current at the inversion point over the peak current is then 92%, whereas the experimental ratio is as low as 50%. It follows that diffusion of $CO_2$ never plays any significant role and therefore that the observed peak shapes do not derive from the interference of this factor.

Another possibility was examined. It consists in considering that $CF_3CH_2OH$ would inactivate $CO_2$, through formation of complexes. This possibility was ruled out by the observation that the $^{13}C$ NMR signal of a 90% $^{13}CO_2$ mixture was not significantly shifted (by <0.05 ppm) by the addition of $CF_3CH_2OH$ up to a concentration of 4.1 M.

Visual observation of the mercury surface at the potential of the catalytic wave under a 300 magnification revealed the formation of an array of CO microbubbles eventually merging into large bubbles which then leave the surface. These microbubbles may reversibly inhibit the reduction of the $Fe(I)^-$ form of the catalyst at the electrode surface. At given scan rate and $CF_3CH_2OH$ concentration, such a self-inhibition

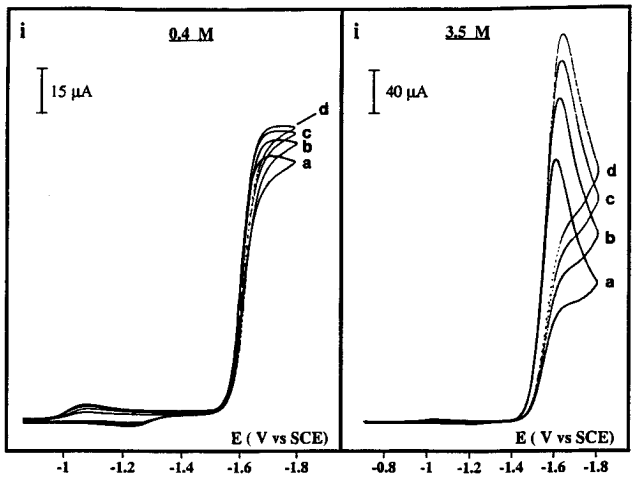


**Figure 7.** Cyclic voltammetry of the reduction of $CO_2$ (1 atm) in DMF + 0.1 M $Et_4NClO_4$ catalyzed by TPPFeCl (1 mM) at two concentrations of $CF_3CH_2OH$ (number on each curve) as a function of the scan rate: (a) 0.1, (b) 0.2, (c) 0.3, and (d) 0.4 V/s. $T$ = 20 °C.

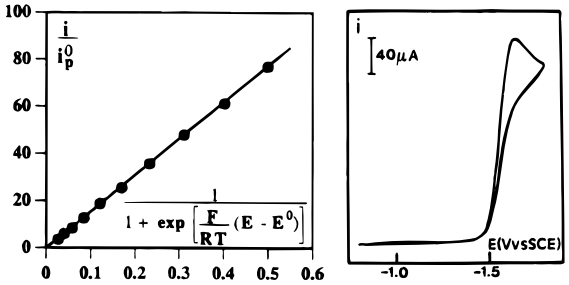


**Figure 8.** Cyclic voltammetry of the reduction of $CO_2$ (1 atm) in DMF + 0.1 M $Et_4NClO_4$ + 1.47 M $CF_3CH_2OH$ catalyzed by TPPFeCl (0.92 mM). Scan rate = 0.1 V/s. $T$ = 20 °C; extraction of the rate constant by application of eq 5.

phenomenon should increase as the potential is scanned along the wave in the negative direction and, as time elapses, thus resulting in the formation of a peak instead of the plateau that is expected in the absence of inhibition. The relative importance of the peak should increase with $CF_3CH_2OH$ concentration, and upon decreasing the scan rate since the formation of CO increases accordingly. These qualitative trends are indeed observed experimentally (Figure 7), and quantitative agreement between theory and experiment can be reached by proper modeling of the self-inhibition phenomenon as discussed later in detail. The model however involves several assumptions whose validity is difficult to assess by independent means. It is thus safer to derive the homogeneous kinetics and from them the reaction mechanism, using the portion of the current−potential curves that is negligibly affected by self-inhibition.

The following strategy was used to reach this goal. Figure 7 shows the variation of the cyclic voltammograms with the scan rate at two concentrations of $CF_3CH_2OH$. At low concentration, the peaks are very flat and an S-shaped curve is obtained at the highest scan rate, in line with the discussion above. Decreasing the scan rate, the peak is more and more pronounced, but there is still a large portion of the cathodic curves which is independent from scan rate and therefore obeys eq 1, describing the voltammogram in the absence of inhibition. The same is true, albeit in a narrower range of potentials, at high $CF_3CH_2OH$ concentration where the peaks are more pronounced (Figure 7). The procedure illustrated in Figure 8 ensues. Within the potential range where the current is independent from scan rate, $i/i_p^0$ is proportional to $1/\{1 + \exp[(F/RT)(E - E^0)]\}$ as expected from eq 3, a recast version

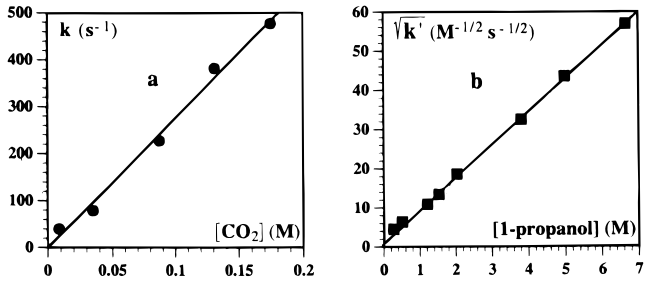


**Figure 9.** Kinetics of the catalysis of $CO_2$ reduction by TPPFeCl (1 mM) in DMF + 0.1 M $Et_4NClO_4$ at 20 °C, variation of the global rate constant with (a) $CO_2$ concentration ([1-propanol] = 6.7M) and (b) 1-propanol concentration under 1 atm of $CO_2$.

of eq 1 in which the current is normalized toward the one-electron catalyst peak current, $i_p^0$.

$$\frac{i}{i_p^0} = \sqrt{\frac{RTk}{F\,v}}\,\frac{2.24}{1+\exp\left[\frac{F}{RT}(E-E^0)\right]} \qquad (3)$$

The rate constant $k$ is derived from the slope of the straight line thus obtained. In the particular case represented in Figure 8, $k = 2.0\ 10^4\ s^{-1}$. This procedure was systematically applied to derive the variations of the global rate constant with $CO_2$ and $CF_3CH_2OH$ concentrations which are those represented in Figure 5. We have already seen that in the range of low $CF_3CH_2OH$ concentrations, where self-inhibition is weak, the kinetic and preparative-scale electrolysis results are consistent with the mechanism depicted in Scheme 1. It is also consistent with the kinetic data for higher concentrations as represented in Figure 5b which have been freed from the effect of self-inhibition by the procedure just described. The tendency of the $k-[CF_3CH_2OH]$ curve to level off at high values of $[CF_3CH_2OH]$ can indeed be explained by the acceleration of steps 2 and 3 which eventually shifts the rate control to forward step 1. In other words, the global rate constant can be expressed as:

$$\frac{2}{k} = \frac{1}{K_1K_2K_3k_4[CO_2][AH]^2} + \frac{1}{k_1[CO_2]} \qquad (4)$$

The solid line in Figure 5b represents the fitting of the data with:

$$K_1K_2K_3k_4 = 2.5\ 10^4\ M^{-3}\ s^{-1},\ k_1 = 7.5\ 10^5\ M^{-1}\ s^{-1}$$

The cyclic voltammetric results obtained with 1-propanol are simpler in the sense that they show almost no peak, and therefore the global rate constant, $k$, can be directly obtained from the plateau currents using eq 1. The variations of $k$ with the concentration of $CO_2$ are displayed in Figure 9a showing that the reaction order in $CO_2$ is 1. From the variations of $k$ with the 1-propanol concentration and the previously determined $CO_2$ solubilities in DMF−1-propanol mixtures,[16] one obtains the pseudo-second-order rate constant $k' = k/[CO_2]$ as a function of 1-propanol concentration (Figure 9b). It is thus found that the reaction order in 1-propanol is 2 and that $K_1K_2K_3k_4 = 74\ M^{-3}\ s^{-1}$. The synergistic effect of 1-propanol is thus substantially (340 times) smaller than that of $CF_3CH_2OH$. This observation explains why self-inhibition does not interfere significantly even at very high concentrations of 1-propanol (6.7 M).

There is however a complicating factor in the case of 1-propanol, namely, that formic acid is produced in significant amount (ca. 30%) besides carbon monoxide. Since the formation of formic acid does not alter the kinetics of the whole reaction, we are led to conclude that it follows the same kinetic law as the formation of CO, namely, that the reaction orders for this process are 1 in $CO_2$ and 2 in 1-propanol. These observations imply that the representation of the various complexes between iron and $CO_2$ by a single resonant form as depicted in Scheme 1 is oversimplified. In Scheme 3, we propose a representation which includes an iron(I)−anion radical structure, besides the iron(II)−carbene resonant structure already considered. The initial adduct formed in reaction 1 would then be hydrogen bonded by one alcohol molecule (reaction 2) as in Scheme 1. The next reactions (3 and 4) leading to the main product, CO, would also be the same, but H-bonding by a second alcohol molecule (reaction 3) would then compete with a reaction (3′) where the singly H-bonded adduct would dissociate into $Fe(I)^-$ and one molecule of H-bonded $CO_2$ anion radical. Following an uphill reversible electron transfer between the two latter species (3″), protonation of the H-bonded dianion would finally leads to formic acid. In the framework of such a mechanism, the difference of behavior between 1-propanol and $CF_3CH_2OH$ can be explained by the lesser ability of the former to provide H-bonding than the latter. 1-Propanol is thus able to form a first hydrogen bond (reaction 2) but is not able to H-bond the resulting less accepting complex (reaction 3) to a sufficient extent to avoid its dissociation (reaction 3′). Confirming these views is the observation that addition of water, an H-bonding agent stronger than 1-propanol, increases the yield in CO at the expense of formic acid.

**Scheme 3**

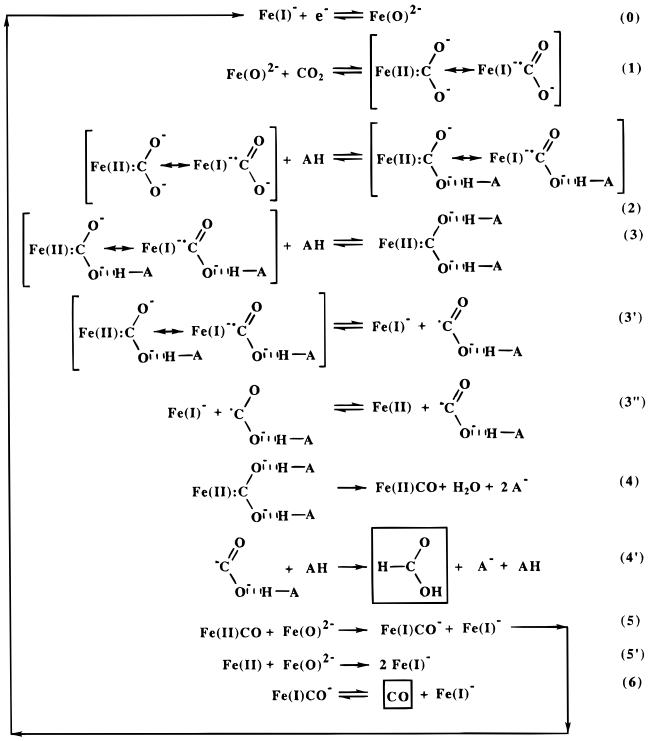


Turning back to preparative-scale electrolysis in the presence of $CF_3CH_2OH$ or 1-propanol, we may estimate the turnover numbers per hour that should have been obtained on the basis of the rate data derived from the cyclic voltammetric experiments if the potential of the working electrode would uniformly sit on the plateau of the wave. These are found to be 350 (CO) for $CF_3CH_2OH$ and 38 (CO) and 18 (formic acid) for 1-propanol, in the conditions of Figure 3a,b, respectively. These values are significantly less than those actually found (see Figure 3a,b) pointing to the interference of ohmic drop which makes

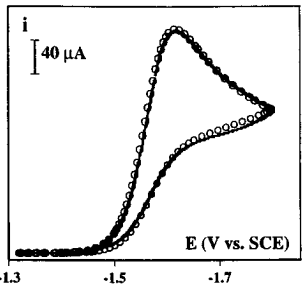


**Figure 10.** Self-inhibited current−potential curve for the catalysis of $CO_2$ (0.23 M) reduction by TPPFeCl (0.75 M) in the presence of 3.48 M $CF_3CH_2OH$ in DMF + 0.1 M $Et_4NClO_4$ at a mercury electrode. $T$ = 20 °C. Scan rate = 0.1 V/s; (—) experimental curve and (○) simulated curve (see text).

the actual electrode potential nonuniformly less negative than the nominal electrode potential. It thus appears that optimization of the cell geometry would lead to substantial improvements of the turnover numbers per hour.

**Self-Inhibition.** The self-inhibition phenomenon observed with $CF_3CH_2OH$ at high catalytic efficiencies can be modeled as follows. The product (CO) of catalysis formed in a thin reaction layer adjacent to the electrode surface may diffuse toward the solution and also to the electrode surface where its adsorbs reversibly. Adsorption and desorption are regarded as fast, and the adsorption equilibrium is assumed to obey the Langmuir law. The adsorbed product is assumed to be randomly distributed over the surface and the portions of the surface that are thus covered to be totally inactive toward the reduction of the catalyst. As shown in detail elsewhere,[19] the inhibited current is given by eq 5 where $\theta$, the relative coverage of the surface by the inhibiting product, is itself obtained from eq 6.

$$\frac{i}{FSC^0D^{1/2}k^{1/2}} = \frac{1-\theta}{1+\exp\left[\frac{F}{RT}(E-E^0)\right]} \qquad (5)$$

$$-\ln(1-\theta) + \frac{1}{K_a}\left(\frac{RTD_{prod}}{F\upsilon}\right)^{1/2}\frac{1}{\pi^{1/2}}\int_0^{\frac{F\upsilon t}{RT}}\frac{\theta}{(1-\theta)\left(\frac{F\upsilon t}{RT}-\eta\right)^{1/2}}\,d\eta = \frac{RTC^0}{F\upsilon\Gamma^0}(kD)^{1/2}\frac{1}{\pi^{1/2}}\int_0^{\frac{F\upsilon t}{RT}}\frac{d\eta}{1+\exp\left[\frac{F}{RT}(E(\eta)-E^0)\right]} \qquad (6)$$

(during the cathodic scan, $E = E_i - \upsilon t$, and during the reverse scan, $E = 2E_f - E_i + \upsilon t$).

Comparison between experiment and the predictions of the model are illustrated in Figure 10 with the cyclic voltammogram obtained at high concentration of $CF_3CH_2OH$ and at a low scan rate where inhibition is maximal. Systematic variations of the two dimensionless parameters contained in eq 6 allowed the determination of a couple of values, $K_a(F\upsilon/RTD_{prod})^{1/2} = 1.02$ and $(RT/F\upsilon)(C^0/\Gamma^0)(kD)^{1/2} = 1.34$, for which the agreement between the experimental and simulated voltammograms is excellent (Figure 10). Further validation of the model is obtained from the comparison of the effect of the scan rate on the self-inhibited experimental curves with the predictions of the theory. In this purpose, the values of $K_a(F/RTD_{prod})^{1/2}$, 3.23 $V^{-1/2}$ $s^{1/2}$, and of $(RT/F)(C^0/\Gamma^0)(kD)^{1/2}$, 0.134 $V^{-1}$ s, were derived from the fitting represented in Figure 10. As seen in Figure 11, there is again an excellent agreement between experiment and theory.

(19) Bhugun, I.; Savéant J.-M. *J. Electroanal. Chem.* in press.

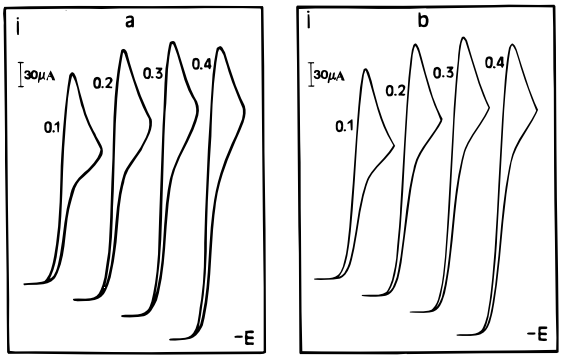


**Figure 11.** Effect of scan rate on self-inhibition in the catalysis of $CO_2$ (0.23 M) reduction by TPPFeCl (0.75 M) in the presence of 3.48 M $CF_3CH_2OH$ in DMF + 0.1 M $Et_4NClO_4$ at a mercury electrode. $T$ = 20 °C. The numbers on the curves are the scan rates in V/s: (a) experimental curves and (b) simulated curves (see text).

## Conclusions

Adddition of weak Brönsted acids such as 1-propanol, 2-pyrrolidone, and $CF_3CH_2OH$ considerably improve the catalysis of $CO_2$ reduction by iron(0) tetraphenylporphyrin in terms of both efficiency and life time of the catalyst without significant formation of hydrogen. Turnover numbers as high as 350/h could be reached with optimized cells where IR drop would be minimized. Carbon monoxide is the major product but not the only product as is the case with $CF_3CH_2OH$. Analysis of the reaction kinetics suggests a mechanism where the first step is the formation of an iron-$CO_2$ adduct whose main resonant form is a $Fe^{II}CO_2^{2-}$ complex. This adduct is stabilized by H-bonding with two acid synergist molecules. The resulting complex is then more prone to cleave one of the C−O bonds than the initial adduct, thus leading to the formation of a CO molecule in the coordination sphere of the iron(II) porphyrin. Reduction of the later complex closes up the catalytic loop. A minor contibutor in the electronic structure of the initial and H-bonded iron−$CO_2$ adducts is a $Fe^{I}-CO_2^{-}$ resonant form. This explains why decomposition of the H-bonded iron−$CO_2$ adduct may thus lead to the formation of formic acid as a minor product along a reaction pathway where the iron−$CO_2$ interactions are weaker than in the main pathway leading to CO. This occurs when the H-bonding ability of the acid synergist is weak as with 1-propanol. It is noteworthy that not only no formate is found with the stronger acid synergist $CF_3CH_2OH$ but also that addition of water decreases the CO yield at the expense of formate. The latter observation is indeed rather counterintuitive in view of the quantitative formation of formic acid upon direct electrolysis in water at an inert electrode.

These findings offer a striking example of the importance of electrophilic assistance in the chemical catalysis of electrochemical reduction. Delivery of two electrons in the coordination sphere of the catalyst is a necessary ingredient of a successful catalysis. Pushing the two electrons into the substrate is however not sufficient. They must then be pulled out by the action of the acid synergist.

With high concentrations of $CF_3CH_2OH$, catalysis becomes so strong that the product, CO, inhibits the reduction of the catalyst. This self-inhibition phenomenon can be satisfactorily modeled considering that product adsorption on the electrode surface obeys a Langmuir equilibrium and that the portions of the surface that are covered are totally inactive toward reduction of the catalyst.

## Experimental Section

**Cyclic Voltammetry.** The working electrode was a mercury drop hung to a 1 mm diameter gold disk, the counter electrode a 1 mm

diameter gold wire, and the reference electrode a NaCl-saturated aqueous saturated calomel electrode. The volume of the solution was 3−5 mL, and the cell was double-jacketed so as to maintain the solution at a fixed temperature, 20°C, by means of a water circulation connected to a thermostat. An Alphagaz Air Liquide mass flow regulator was used for the reduced $CO_2$ pressure experiments. The potentiostat and the current measurer, implemented with a positive feedback ohmic drop compensation, were home-built instruments.[20] They were used together with a EGG PAR 175 signal generator and a IFELEC 2502 chart recorder. Because the reduction wave of $TPPFe^{III}Cl$ is merged with the mercury oxidation current, the starting potential was positioned in the range of stability of Fe(II) and the scan started after stabilization of the current. The same electrodes and potentiostat were used for visual observation of the working electrode at the potential of the catalytic wave, but the cell was replaced by a thin layer cell and the working electrode was positioned in between the two parallel glass windows.

**Preparative-Scale Electrolyses.** The same gas expansion cell as described earlier[3b] was used in all preparative scale experiments. The working electrode was a 10 $cm^2$ circular mercury pool whose surface was constantly renewed by means of a magnetic stirrer. In order to avoid contamination by water during electrolysis (several hours), we did not use an aqueous saturated calomel electrode as reference electrode but rather a cadmium amalgam electrode ($Cd/CdHg/CdCl_2$) in DMF[21] separated from the cathodic compartment by a bridge containing a 0.1 M $Et_4NClO_4$ DMF solution. The potential difference with the aqueous SCE, ca. 0.73 V, can be checked potentiometrically when required. The counter electrode was a platinum wire in a bridge separated from the cathodic compartment by a glass frit and containing a 0.4 M $Et_4NO_2CCH_3$ + 0.1 M $Et_4NClO_4$ DMF solution. $CO_2$ and ethane are produced at this electrode (Kolbe reaction) during electrolysis. All electrolyses were carried out in a glovebox so as to minimize side reactions triggered by the presence of dioxygen and/or water.

The potentiostat (50 V, 1 A) was a home-built instrument. The charge passed was measured with a IGN5 Taccussel integrator.

The volumes of the solution and gas phase were 17 and 39 mL, respectively. The two phases were analyzed separately during each electrolysis, and the fate of the porphyrin catalyst was followed by cyclic voltammetry on a microelectrode introduced in the cell.

$H_2$, CO, $CH_4$, and $CO_2$ were sought in samples of the gas phase extracted with a Hamilton tight-gas syringe and titrated by gas chromatography when found. The chromatograph was a GC-14B instrument with thermal conductivity detection equipped with a 2.2 mm diameter/2 m length column containing a 80/60 Carbosieve S stationary phase. The operating conditions were as follows: vector gas, helium (2 bars of input pressure); oven temperature, 85 °C; injected volume, 0.2 mL; analysis time, 16 min. Quantitative analysis used an external calibration, carried out the same day, based on the peak surface areas of volumes of the pure gas comprised between 0.01 and 0.2 mL. Under these conditions, the peak surface areas are proportional to the injected volumes.

Formate and oxalate were identified and titrated by ionic chromatography. The chromatograph was a DX-100 Dionex instrument equipped with a conductimetric detector and a 4 mm conductivity suppressor (AsRS-I). A 4 mm diameter Dionex IonPac AS10 column was used to separate the anions. The operating conditions were as follows: mobile phase, 65 mM NaOH in ultrapure water with a flow rate of 1 mL/min; injection volume, 100 $\mu$L; analysis time, 20 min. The quantitative analyses were carried out after dilution of 0.2 mL of the electrolyzed solution into 100 mL of ultrapure water followed by filtration through a 0.5 $\mu$m Millipore filter. The purpose of this pretreatment is to eliminate the porphyrin by precipitation and dilute both DMF and $Et_4NClO_4$ which could perturb the analysis if present in high concentrations. The titration was then performed with an external calibration, carried out the same day, based on the peak surface areas of known volumes of standard solutions of sodium formate or oxalic acid (concentration, 0.3−3 ppm). Under these conditions, the peak surface areas are proportional to the injected concentrations.

Analysis of formaldehyde was based on the formation of a colored product upon reaction with chromotropic acid (Merck Spectroquant kit, with visible spectrophotometric detection at 570 nm). The electrolyzed solutions were first pretreated as for formate and oxalate except that dilution was 50 times instead of 500 times. The external calibration was carried out with concentrations ranging from 0.25 to 1.5 mM.

Methanol was sought by gas chromatography with the same instrumentation as used for gas analyses except that the stationary phase was 60/80 Porapak Q. The operating conditions were as follows: vector gas, helium (2 bars of input pressure); oven temperature, 120 °C during 6 min followed by a 30 °C/min linear increase up to 150 °C' injected volume, 1−2 $\mu$L; analysis time, 25 min. The electrolyzed solutions were injected without pretreatment, and the chromatogram was compared to a standard solution containing 0.5 mM methanol, i.e., ca. 1% of the total conversion faradaic yield.

**$^{13}$C NMR.** The reference solution, 90% $^{13}$C-enriched $CO_2$ in DMF, showed a signal at 125.25 ppm vs tetramethylsilane. $CF_3CH_2OH$ was added to the solution up to 40% in volume.

**Chemicals.** Their origin and characteristics were as follows. The gases were from Air Liquide:argon (U), helium (N55), hydrogen (U), methane (N45), CO (N47), $CO_2$ (N45), and 90% $^{13}$C-enriched $CO_2$ from Eurositop. DMF was from Fluka, Burdick and Jackson, high purity grade, kept under argon. Water was obtained from a Millipore Milli-Q Plus system. 1-Propanol, $CF_3CH_2OH$, and 2-pyrrolidone were from Aldrich (≥99%). $Et_4NClO_4$ was a Fluka purum product. It was recrystallized these times in a 2−1 ethanol−ethyl acetate mixture at 95 °C before use. TPPFeCl and $Et_4NO_2CCH_3 \cdot 5H_2O$ were Aldrich products. Sodium formate was from Fluka (microselect, ≥99.5%) and oxalic acid from Merck (Suprapur). Mercury, first washed with 5% nitric acid (Merck, Suprapur), was vacuum-distilled twice. Anodic stripping measurements in ultrapure KCl or $KNO_3$ solutions showed the absence of heavy metals (Cu, Ni, Pb, Cd, Zn). It was kept under an inert atmosphere and paper-filtered before use.

**Acknowledgment.** We are grateful to Dr. J. Chevalet for the gift of purified mercury used as electrode in this study.

**Supporting Information Available:** Further reactions for Schemes 1 and 2 (3 pages). This material is contained in many libraries on microfiche, immediately follows this article in the microfilm version of the journal, can be ordered from ACS, and can be downloaded from the Internet; see any current masthead page for ordering information and Internet access instructions.

JA9534462

(20) Garreau, D.; Savéant, J.-M. *J. Electroanal. Chem.* **1972**, *35*, 309.
(21) Andrieux, C. P.; Delgado, G.; Savéant, J.-M.; Su, K. B. *J. Electroanal. Chem.* **1993**, *348*, 107.